

Reactive Flow Modeling of the Interaction of TATB Detonation Waves with Inert Materials

C.M. Tarver, E.M. McGuire

This article was submitted to
12th International Detonation Symposium, San Diego, California,
August 11-16, 2002

U.S. Department of Energy

July 1, 2002

Lawrence
Livermore
National
Laboratory

DISCLAIMER

This document was prepared as an account of work sponsored by an agency of the United States Government. Neither the United States Government nor the University of California nor any of their employees, makes any warranty, express or implied, or assumes any legal liability or responsibility for the accuracy, completeness, or usefulness of any information, apparatus, product, or process disclosed, or represents that its use would not infringe privately owned rights. Reference herein to any specific commercial product, process, or service by trade name, trademark, manufacturer, or otherwise, does not necessarily constitute or imply its endorsement, recommendation, or favoring by the United States Government or the University of California. The views and opinions of authors expressed herein do not necessarily state or reflect those of the United States Government or the University of California, and shall not be used for advertising or product endorsement purposes.

This is a preprint of a paper intended for publication in a journal or proceedings. Since changes may be made before publication, this preprint is made available with the understanding that it will not be cited or reproduced without the permission of the author.

This report has been reproduced directly from the best available copy.

Available electronically at <http://www.doe.gov/bridge>

Available for a processing fee to U.S. Department of Energy
and its contractors in paper from
U.S. Department of Energy
Office of Scientific and Technical Information
P.O. Box 62
Oak Ridge, TN 37831-0062
Telephone: (865) 576-8401
Facsimile: (865) 576-5728
E-mail: reports@adonis.osti.gov

Available for the sale to the public from
U.S. Department of Commerce
National Technical Information Service
5285 Port Royal Road
Springfield, VA 22161
Telephone: (800) 553-6847
Facsimile: (703) 605-6900
E-mail: orders@ntis.fedworld.gov
Online ordering: <http://www.ntis.gov/ordering.htm>

OR

Lawrence Livermore National Laboratory
Technical Information Department's Digital Library
<http://www.llnl.gov/tid/Library.html>

REACTIVE FLOW MODELING OF THE INTERACTION OF TATB DETONATION WAVES WITH INERT MATERIALS*

Craig M. Tarver and Estella M. McGuire
Lawrence Livermore National Laboratory
Livermore, CA 94551

The Ignition & Growth model for the shock initiation and detonation of solid explosives is applied to calculating the main features of detonation waves in the triaminotrinitrobenzene (TATB) based high explosives LX-17, PBX 9502 and EDC-35. Under detonation conditions, TATB based explosives exhibit reaction zone lengths of 2 to 3 mm depending on the interactions between the detonation wave and the surrounding inert materials. This paper describes comparisons of Ignition & Growth calculations with data from several two- and three-dimensional experiments in which various materials are used to confine the TATB based explosives. The calculated unconfined failure diameters of PBX 9502 are normalized to the measured values at five initial temperatures. Failure diameters for LX-17 are then estimated by changing only the fraction ignited near the shock front. Fabry-Perot data on spherically divergent LX-17 snowball experiments is also compared to calculations. Calculated detonation velocities, wave front curvatures, and metal acceleration velocities are compared to experimental detonation data for TATB-based high explosives in tantalum, copper, PMMA, brass, and beryllium confinement. Three-dimensional prism failure test results on PBX 9502 are also stimulated using the ALE3D code.

INTRODUCTION

Triaminotrinitrobenzene (TATB) - based solid explosives are widely used due to their excellent safety characteristics. Three high density versions are: LX-17 (92.5% TATB/7.5% K₂FeF₆); PBX 9502 (95% TATB/5% K₂FeF₆); and EDC-35 (95% TATB/5% K₂FeF₆). These explosives exhibit 2 to 3 mm reaction zone lengths and many non-ideal propagation properties when detonating.¹ The Ignition & Growth reactive flow model has been applied to a great deal of experimental data on TATB detonation waves in order to predict this non-ideal behavior in geometries that can not be tested. Numerous one-dimensional embedded gauge and laser interferometer experiments on detonating LX-17 and PBX 9502 have created an excellent database for reactive flow modeling.² Various two-dimensional experiments have shed considerable light on the detonation versus charge diameter, failure diameter, and wave curvature properties of detonating TATB.³ The three-dimensional prism failure test⁴ has also provided an excellent test for TATB reactive flow modeling. In

this paper, several of the most interesting two- and three-dimensional experiments on these three TATB-based explosives are described and calculated. The results are used to determine the ability of the model to predict a wide range of confinement effects ranging from no confinement (failure diameter cylindrical rate sticks and spherical divergence) to medium confinement (PMMA and beryllium cylinders) to heavy confinement (brass, steel, copper, and tantalum cylinders).

IGNITION & GROWTH MODEL

The Ignition and Growth reactive flow model of shock initiation and detonation of solid explosives has been incorporated into several hydrodynamic computer codes and used to solve many 1D, 2D, and 3D explosive and propellant safety and performance problems.⁵⁻¹¹ The model uses two Jones-Wilkins-Lee (JWL) equations of state, one for the unreacted explosive and one for its reaction products, in the temperature dependent form:

$$p = A e^{-R_1 V} + B e^{-R_2 V} + \omega C_V T / V \quad (1)$$

where p is pressure in Megabars, V is relative volume, T is temperature, ω is the Gruneisen coefficient, C_v is the average heat capacity, and A , B , R_1 , and R_2 are constants. The reaction rate law for the conversion of explosive to products is:

$$\begin{aligned} dF/dt = & I(1-F)^b(\rho/\rho_0-1-a)^x + G_1(1-F)^c F^d p^y \\ & (0 < F < F_{igmax}) \quad (0 < F < F_{G1max}) \\ & + G_2(1-F)^e F^g p^z \quad (F_{G2min} < F < 1) \end{aligned} \quad (2)$$

where F is the fraction reacted, t is time, ρ is the current density, ρ_0 is the initial density, and I , G_1 , G_2 , a , b , c , d , e , g , x , y , and z are constants. The mixture equations assume pressure and temperature equilibration between the unreacted explosive and its reaction products.

This three-term rate law describes the three stages of reaction generally observed in shock initiation and detonation of heterogeneous solid explosives. For detonation, the first term represents the ignition of the explosive as it is compressed by the leading shock wave creating heated areas (hot spots) as the voids in the material collapse. The fraction of explosive ignited is approximately equal to the original void volume.⁵ The second reaction models the rapid formation of the major reaction product gases (CO_2 , N_2 , H_2O , CO , etc.) in highly vibrationally excited states¹² and their subsequent expansion and equilibration. The third term is used to describe the relatively slow diffusion controlled formation of the solid carbon particles in the form of diamond, graphite, or amorphous carbon. For TATB-based explosives, the last 20% of the energy release is assumed to be solid carbon formation. Other LX-17 and Ultrafine TATB Ignition and Growth applications are shown in companion papers.^{13,14} The mesh sizes used in these calculations are 10 and 20 zones per mm. The results are independent of mesh size so the modeling has converged to consistent answers.

FAILURE DIAMETER RESULTS

The failure diameter of PBX 9502 has been determined at five initial temperatures: -55°C; 24°C; 75°C, 170°C and 250°C. For the first three temperatures, the conventional cylindrical rate stick

measurements of Campbell^{15,16} are used. For the highest two temperatures, the prism test results of Asay and McAfee¹⁷ are used.

An Ignition & Growth reactive flow model for PBX 9502 based on the widely used LX-17 model was developed for the shock initiation embedded gauge experiments of Gustavsen et al.¹⁸ The only changes were to decrease the critical compression [parameter a in Eq. (2)] at which reaction begins from 0.22 for LX-17 to 0.214 for PBX 9502 and to increase the maximum fraction reacted ignited by the first term of Eq. (2) from 0.02 for LX-17 to 0.025 for PBX 9502 (F_{igmax} in Eq. (2)). These two changes are based on the experimental facts that PBX 9502 reacts at slightly lower shock pressures than LX-17 and that PBX 9502 is typically pressed to 97.5% of its theoretical maximum density (TMD), while LX-17 is pressed to 98% TMD. Table 1 contains all of the Ignition & Growth equation of state and reaction rate parameters used for LX-17 and PBX 9502. The calculated failure diameters of PBX 9502 at these five initial temperatures were then normalized to the experimental values by varying G_1 and the pressure exponent y in the second (reaction growth) term of Eq. (2). Growth coefficients G_1 were obtained for both $y=2$ and $y=3$, both of which have been used to model TATB-based reaction rates in previous work.

In unconfined failure diameter calculations, the use of $y=3$ yields relatively fast failure of detonation after a few centimeters of propagation at the limiting experimental detonation velocities (7.4 mm/ μ s for PBX 9502).¹⁶ The use of $y=2$ also yields failure at the correct diameters and velocities, but this failure process requires long distances (20 to 40 cm) of propagation. Experimentally, Campbell¹⁶ has demonstrated that the failure of a PBX 9502 detonation wave in a cylindrical rate stick can take 25 to 30 cm. Therefore using $y=2$ in Eq. (2) is more physically correct, but using $y=3$ yields sharp failure/detonation limits at much shorter run distances. The two pressure dependencies give essentially the same results for all of the experiments discussed in this paper. Table 2 lists the values of G_1 and y used for each initial temperature of PBX 9502, the experimental failure diameter or twice the failure thickness, and calculated failure/detonation diameter. These

calculated values predict failure diameter to within 1 mm, and more exact values could be determined.

The failure diameter of LX-17 has never been determined, but it is assumed to be midway between the 95% TATB/ 5% Kelf and 90% TATB/ 10% Kelf values of Campbell and Engelke.¹⁵ Table 2 contains the calculated failure diameters for LX-17 at —55BC24BC, and 75BC determined by changing only parameters α and Figmax in Eq. (2). Recent work on ambient temperature LX-17 has shown that its failure diameter is very close to the calculated estimate of 11 —12 mm.¹³ It is encouraging that the ignition term of the model is sensitive enough to predict a change in failure diameter of 7 —8 mm for PBX 9502 to 11 —12 mm for LX-17 by just accounting for the differences in porosity. Ignition & Growth predicts the increase in failure diameter as the initial density approaches TMD for LX-17, a well-known phenomenon for carbon rich explosives like TATB and TNT,¹⁹ but more experimentation at higher densities and large diameters is required.¹³ Experiments to determine the failure diameter of LX-17 at —55BC and 75BC are planned to check the predicted failure diameters listed in Table 2.

DIVERGING LX-17 DETONATION WAVES

In a companion paper, Druce et al.¹⁴ present Fabry-Perot velocity history measurements at 5 angles for spherically diverging detonation waves in LX-10 and Ultrafine TATB booster explosives and the corresponding Ignition and Growth reactive flow calculations of the entire experimental geometries. Fabry-Perot experiments have also been fired in which 1.15 cm shells of LX-17 have placed between the Ultrafine TATB boosters and the PMMA windows. These snowball tests measure the breakout times and interface particle velocity histories at 5 β , 30 β , 60 β , 75 β , and 85 β . Figure 1 shows the experimental Fabry-Perot records for three LX-17 snowball tests and the Ignition & Growth calculations using the LX-17 parameters in Table 1 and the Ultrafine TATB, aluminum, steel, LX-16, PBX 9407, and PMMA parameters given by Druce et al.¹³ The calculated arrival times are in the correct order (60 β , 30 β , 75 β , 7 β , and finally 85 β), and the calculated maximum interface particle velocities for LX-17 impacting PMMA agree well with experiment. These particle velocities have not reached the C-J values for LX-17, thereby indicating

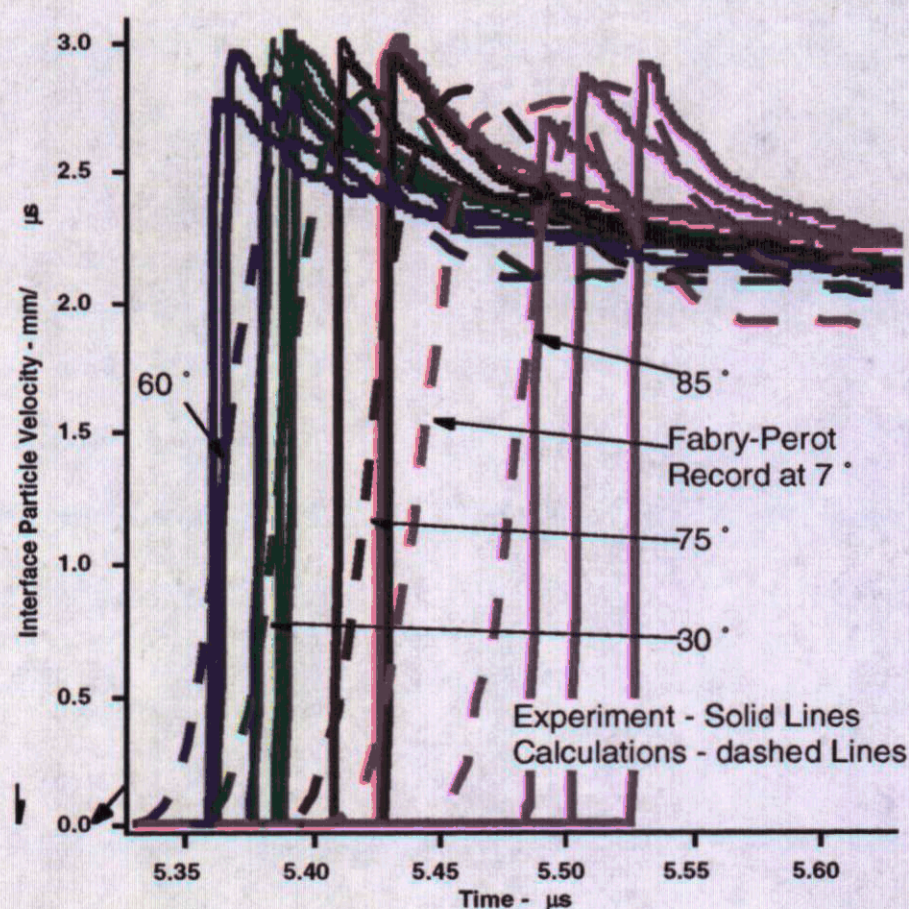


Figure 1. Experimental and Calculated Interface Particle Velocity Histories for LX-17 Snowballs and PMMA Windows

that the LX-17 detonation wave is still growing toward its steady state strength. These results agree closely with a previous study by Bahl et al.⁷ in which only one Fabry-Perot beam was available and only the 0 β and 60 β angles were studied. Spherical divergence is one of the most difficult and most important geometries for reactive flow models to predict, and the agreement shown in Fig. 1 is excellent proof of the accuracy of the LX-17 detonation model in that geometry.

CONFINED CYLINDRICAL LX-17 WAVES

LX-17 cylinders have been fired using copper, tantalum, and PMMA tubes. Streak cameras and Fabry-Perot laser interferometry are used to measure the wall velocity histories. Detonation wave curvature measurements were made on the top of the LX-17 charges in the case of copper and PMMA. Several copper cylinder tests were fired using 2.5417 cm radius LX-17 cylinders confined by 0.2721 cm thick copper tubes. The Fabry-Perot records for one of these shots showed evidence of spall in the copper tube, while those from the other shots did not. The experiments were modeled using the LX-17 parameters shown in Table 1 and the Steinberg-Guinan model²⁰ with the Gruneisen

parameters listed in Table 3. The spall strength was set equal to -1.8 GPa , as determined for high explosive driven spall in copper discs by Tarver and Maiden.²¹ A second calculation was done with the spall option turned off. Figure 2 shows the Fabry-Perot record and the Ignition & Growth simulation with the spall model off for a copper cylinder test that did not spall, while Fig. 3 shows similar records with the spall model on for the cylinder that did spall. Both calculations agree very well with the tests, except for the initial jump-off velocity. The streak cameras and Fabry-Perot laser interferometers do not resolve this initial velocity well, because of the air shock wave and the early time angle variations of the copper motion. The Fabry-Perot lasers are set at 7β for copper. Ignition & Growth modeling shows that the maximum velocity vector settles down to 7β before the second shock jump but varies significantly at earlier times.

A close examination of the calculated pressure states in the copper walls indicated that the spall criterion is reached only periodically in the wall. So the Fabry-Perot and streak cameras will only record spall-like patterns when they are focused on an area of high tension. Only one of three LX-17/Cu cylinder tests with these dimensions spalled. Spall was only predicted by using both the Ignition & Growth and the Steinberg-Guinan models.

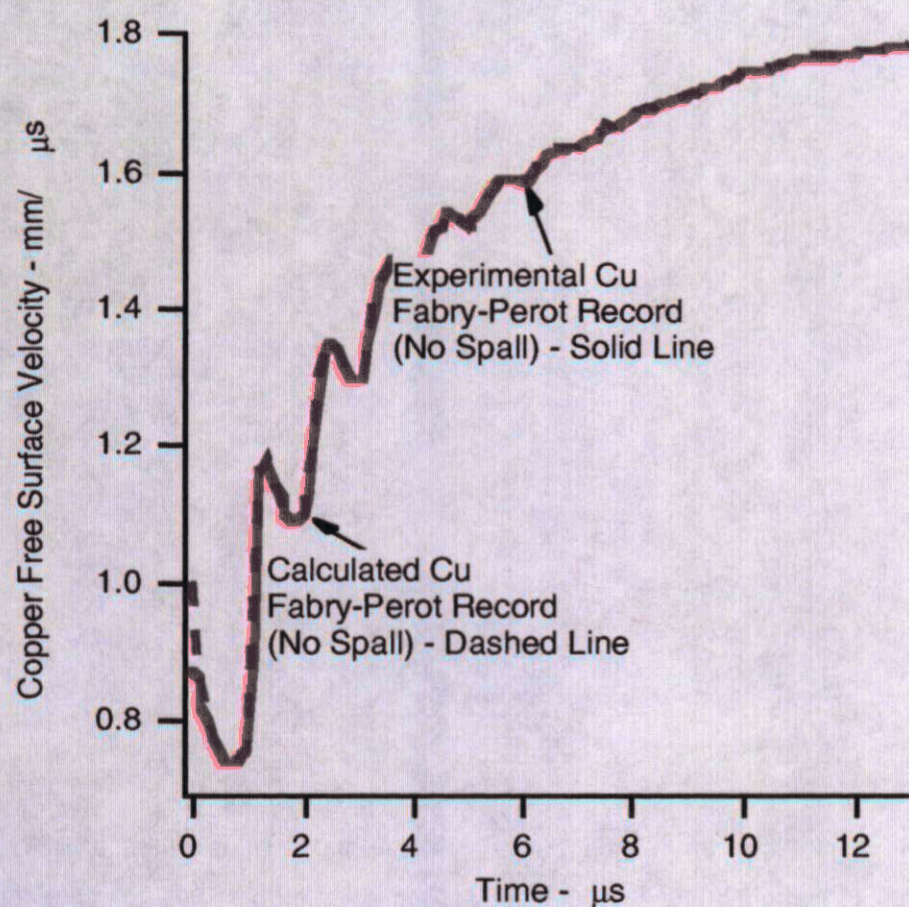


Figure 2. Experimental and Calculated LX-17 Copper Cylinder Test Results without Spall

One tantalum cylinder was fired using LX-17 about 10 years ago.²² The LX-17 radius was 2.5415 cm and the Ta thickness was 0.2717 cm. Figure 4 shows the Ta cylinder Fabry-Perot record and the corresponding Ignition & Growth modeling results.

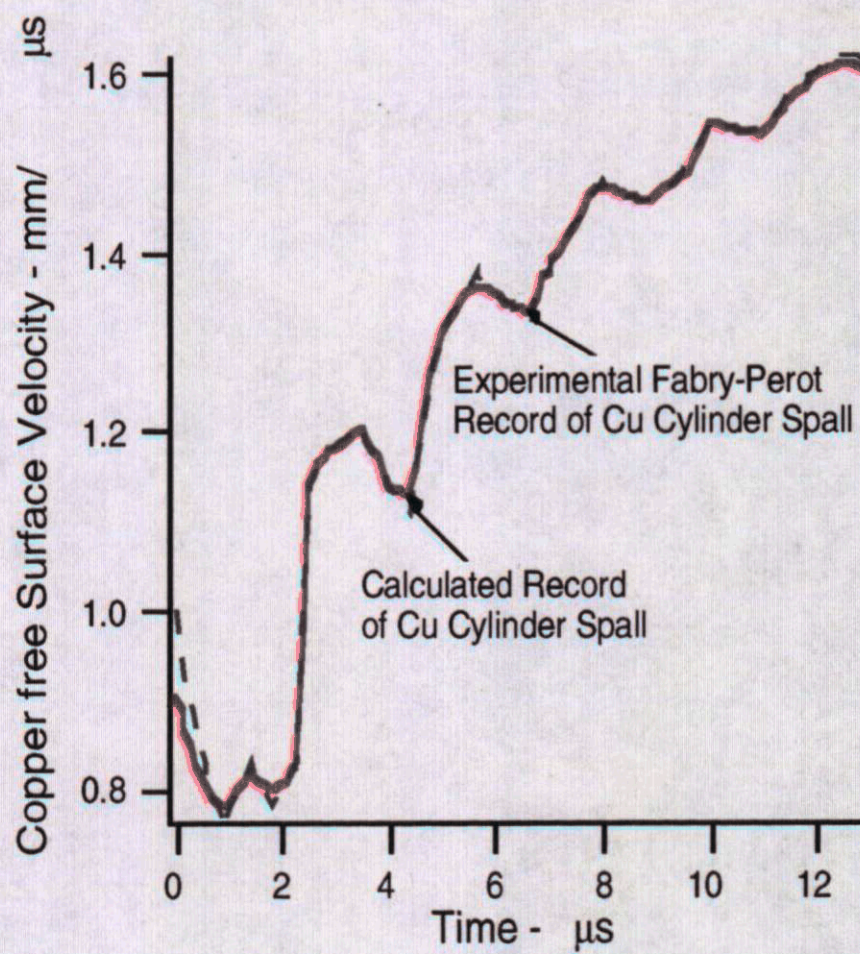


Figure 3. Experimental and Calculated LX-17 Copper Cylinder Test Results with Spall

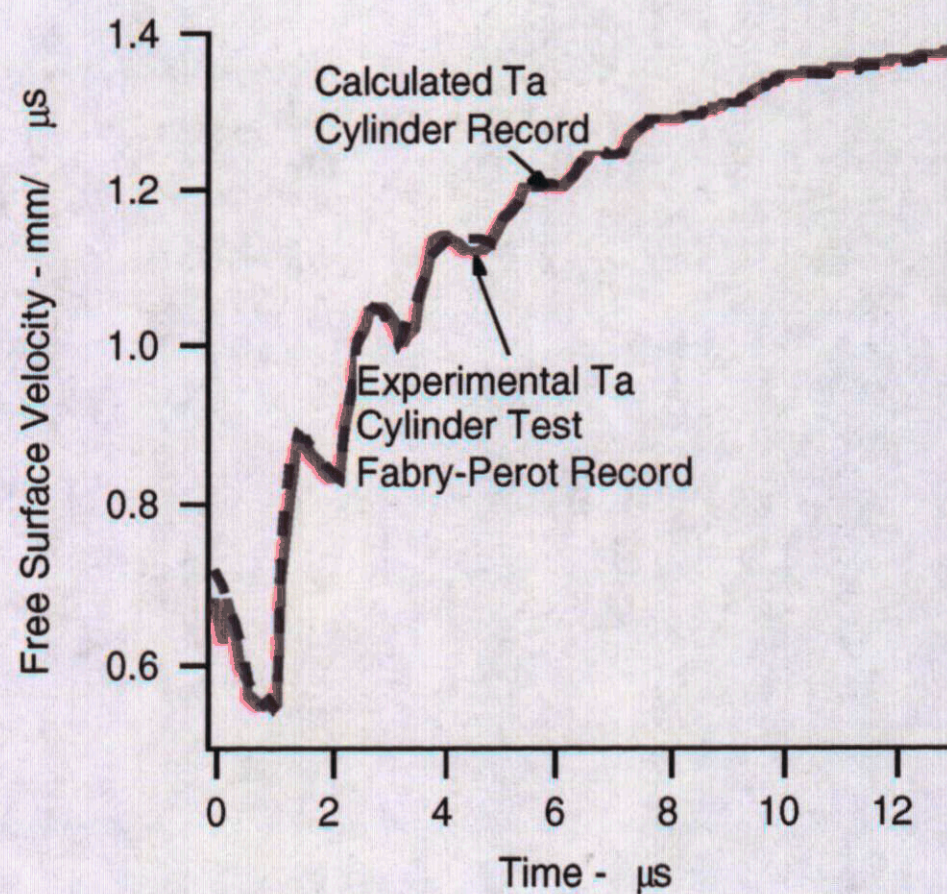


Figure 4. Experimental and Calculated LX-17 Tantalum Cylinder Test Results

The Fabry-Perot angle was set at 5β as determined by the calculations. The agreement is excellent except for the initial jump-off velocity. No evidence of Ta spall was observed experimentally or in the calculated Ta states using the -8.0 GPa criteria for high explosive driven spall.²¹

Recently some LX-17 cylinders were detonated using PMMA confining tubes.²³ The LX-17 radius was 1.27 cm and the PMMA was also 1.27 cm thick. A very thin layer of aluminum was placed on the inner wall of the PMMA cylinder so the Fabry-Perot would record the interface velocity history of the reaction products and the PMMA. Unfortunately, the Fabry-Perot angle was mistakenly set at 7β , while both analytical theory²⁴ and Ignition & Growth calculations showed that the angle should have been set at approximately 35β . Since the cosine of 7β is 0.9925, the Fabry-Perot velocimeters essentially measured the radial component of the interface velocity. In Fig. 5, the average of 9 Fabry-Perot records and the calculated radial velocity for the interface between detonating LX-17 and PMMA are compared for the $0.8 \mu\text{s}$ that the longest experimental records lasted.

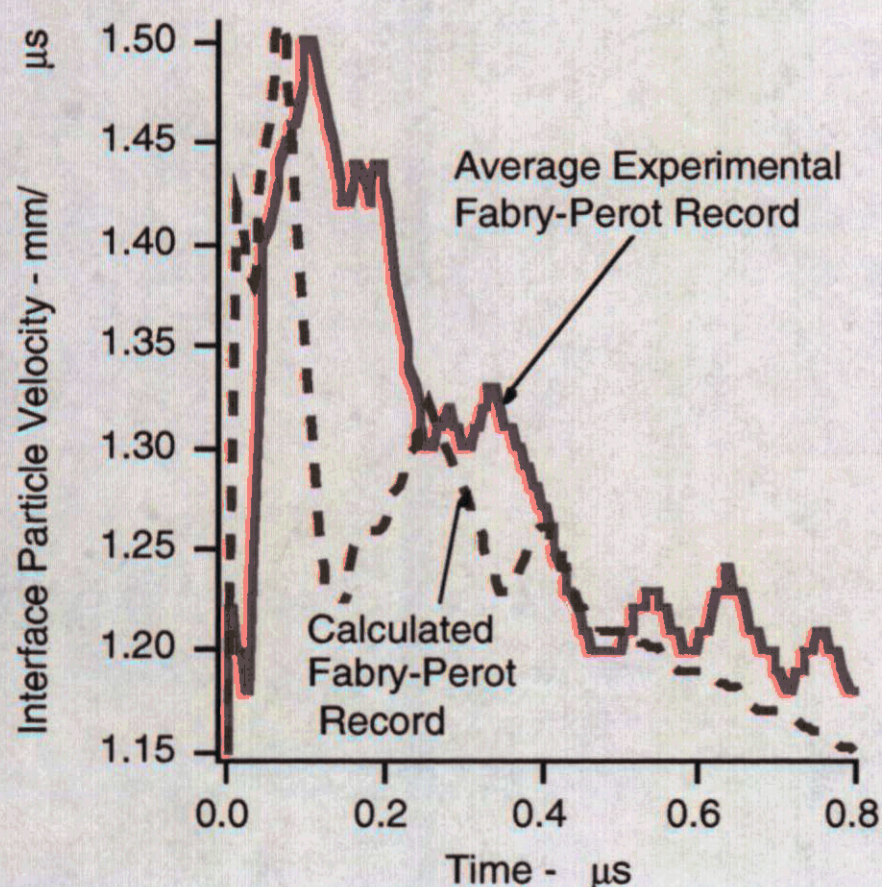


Figure 5. Experimental and Calculated Interface Particle Velocity Histories for LX-17 PMMA Radial Cylinder Test Expansion

The wave curvature at the top of the LX-17 charges was measured for two copper cylinders and a PMMA cylinder. Unfortunately, curvature was not measured for the tantalum cylinder test. Figure 6 contains two experimental wave curvatures for copper and one PMMA and the calculated curvatures for copper, PMMA, and tantalum confinement. Combining this data with that for unconfined LX-17 and LX-17 confined by teflon shown in a companion paper,¹³ the LX-17 reactive flow models calculated wave curvatures are very close to experiment for a wide range of confinement strengths. Thus the LX-17 model yields excellent descriptions of the curved detonation wave front and inert material acceleration in cylindrical geometry.

THE INTERACTION OF EDC35 WAVES WITH BRASS AND BERYLLIUM WALLS

Eden and Belcher²⁵ reported an excellent study of the effects of brass and beryllium walls on the propagation velocity of detonating 25 mm thick slabs of EDC35. The EDC35 slabs were initiated by 25 mm square cross section Composition B boosters. The brass plates were 10 mm thick, while the beryllium plates were 9.3 mm thick. The arrival times were measured at 20, 40, 60, 80, and

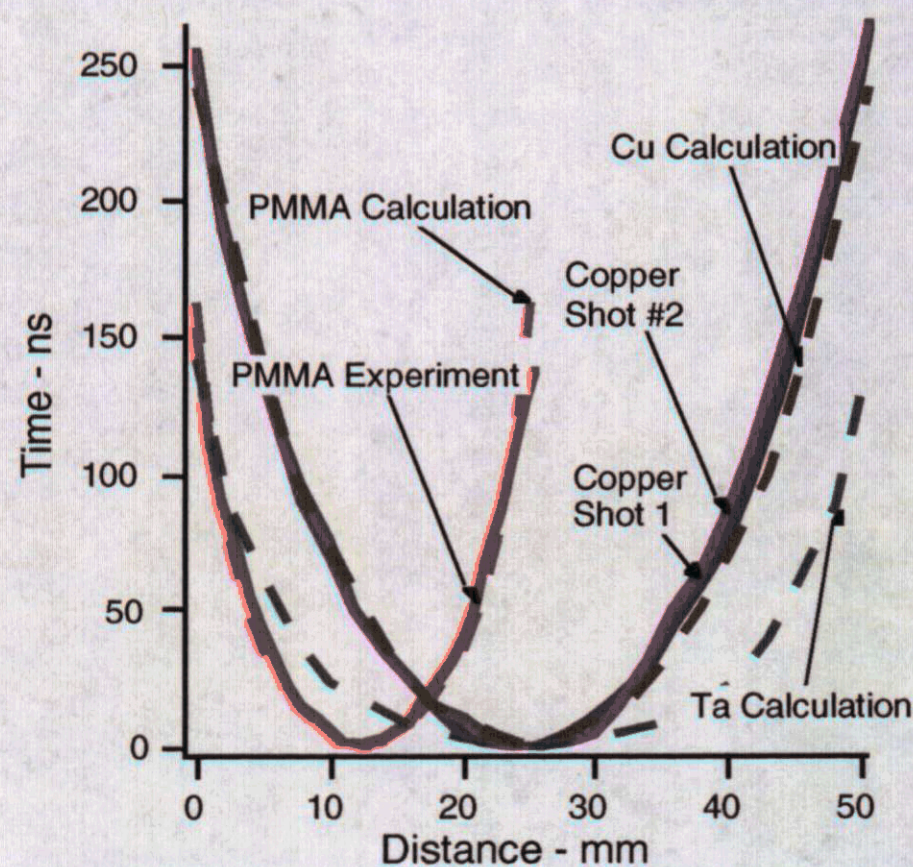


Figure 6. Experimental and Calculated LX-17 Detonation Wave Curvature for PMMA, Copper, and Tantalum Cylinders

100 mm of EDC35 detonation wave propagation along the beryllium interface and at the corresponding positions in the brass. Like copper, tantalum, and PMMA, brass has a lower shock velocity than the EDC35 detonation velocity, and normal curved front patterns like those in Fig. 6 are observed. However, beryllium has a higher shock velocity than the EDC35 detonation velocity and therefore pulls the detonation wave along at higher than normal detonation velocities at the EDC35-Be interface. An Ignition & Growth calculation was done of the entire experiment using the PBX 9502 parameters in Table 1 for EDC35, a C-J detonation model for Composition B shown in Table 4, and the brass and beryllium parameters shown in Table 3. This calculation reproduced all of the effects observed experimentally: an elastic wave in Be traveling at over 12 km/s; a slower propagation of the EDC35 wave along the brass surface; a faster propagation along the Be surface; and even a weak shock moving at about 3 km/s with about 3 GPa pressure connecting the EDC35 wave to the Be shock front. Table 5 shows the comparisons of the experimental and calculated arrival time differences at the 5 measurement distances and the average propagation velocities of the EDC35 detonation wave along the two inert surfaces. The agreement between the Ignition & Growth predictions and the experimental results is excellent. The model predicts slightly faster propagation along the Be than observed experimentally and thus slightly greater timing differences between the brass and Be arrival times. Figure 7 shows the EDC35 detonation wave pressure contours at 18.676 μ s at breakout of the leading detonation front after 100 mm of propagation with the leading Be shock on the right side and the lagging brass shock front on the left. This snapshot is very similar to the experimental records of Eden and Belcher.²⁵ Thus the model did an excellent job of simulating the effect of the Be wall on the propagation of an EDC35 detonation.

THREE-DIMENSIONAL PRISM FAILURE TEST MODELING FOR PBX 9502

The three-dimensional prism test for detonation failure developed by Ramsay⁴ is an excellent test of the PBX 9502 reactive flow parameters. In this test, a detonation wave is initiated with a 150 mm long line-wave generator into a 12 x 12 x 150 mm

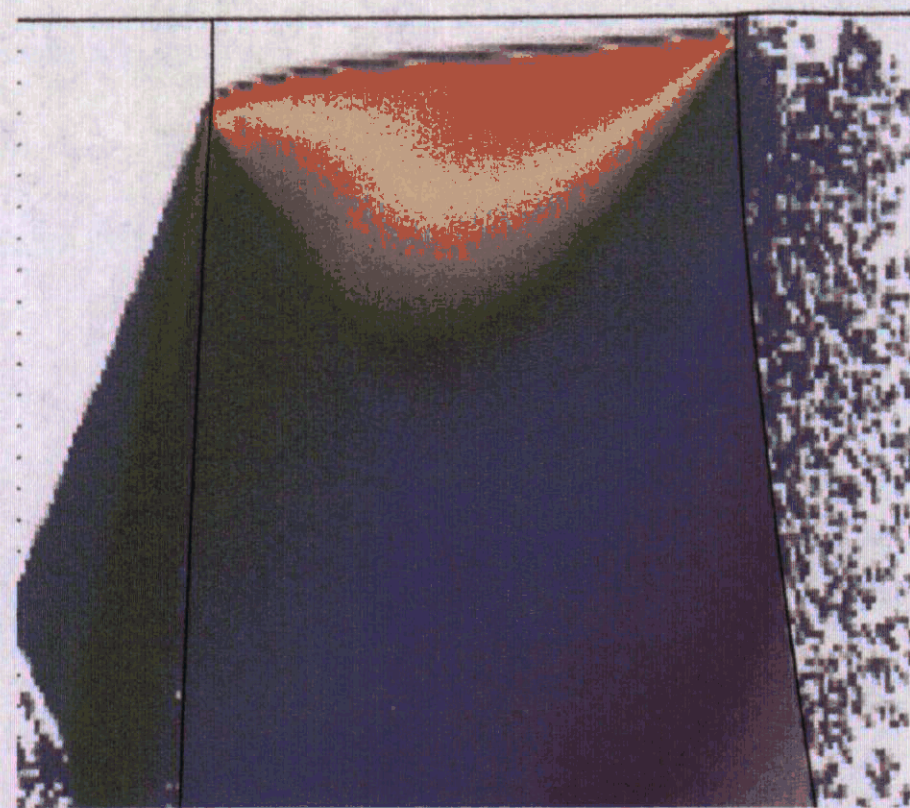


Figure 7. Pressure Contours for an EDC-35 Detonation Wave after 100 mm of Propagation along of Brass Confinement (left side) and Beryllium Confinement (right side)

booster of PBX 9501 (95wt% HMX/ 5%estane-plasticizer binder). This detonation wave travels into a 12 x 12 x 150 mm booster of PBX 9502 and then into a 150 mm long, 50 mm wide wedge of PBX 9502 with a 2 β taper. The base of the wedge was 8 mm thick and the toe 2 mm thick for most shots. The thickness at the point of detonation failure is measured from the dent formed in a dural witness plate. An experiment using two PBX 9502 prisms edge-to-edge provided a total run distance of 100 mm and showed that the prism failure thickness is very close to 1/2 of the cylindrical rate stick failure diameter. Various inert materials were used to confine the PBX 9502 prisms and reduce the failure thicknesses.⁴ Asay and McAfee¹⁷ used the prism test to estimate the failure diameter of PBX 9502 heated to 170 β C and 250 β C. All of the other experiments modeled in this paper have an axis of symmetry and can be modeled as two-dimensional in the DYNA2D, LS-DYNA2D, and CALE codes. This prism test is truly three-dimensional and must be modeled as such. Three-dimensional meshes of the entire prism test were developed for the LS-DYNA3D and ALE3D codes, which contain identical versions of the Ignition & Growth model. The 3D reactive flow modeling of the prism test

shows that the whole prism face begins to react when hit by the PBX 9502 donor detonation wave. However, this reaction begins to fail almost immediately at the narrow edge of the wedge. The failure of reaction moves inward faster for reaction growth rates that depend upon pressure cubed than for those which depend on pressure squared. This failure of reaction continues until a wedge thickness of approximately 4 mm is reached after 2 to 3 cm of propagation. The PBX 9502 detonation then propagates with small oscillations until the end of 5 cm long wedge is reached. Therefore the calculated failure thickness of unconfined PBX 9502 is very close to the experimental value of 4 mm, which is approximately half of the cylindrical failure diameter. The calculated effects of confinement density and thickness on the prism failure thickness will be compared to experimental measurements in a later paper.

CONCLUSIONS

The LX-17 and PBX 9502 detonation Ignition & Growth reactive flow models were shown to accurately simulate a wide variety of two- and three-dimensional experiments, which used confinements ranging from none to very heavy. They can be used with confidence to predict 2D and 3D detonation propagation in scenarios which can not be tested. Although more sophisticated reactive flow models are being developed,²⁶ the accuracy, flexibility, and wide availability of the Ignition & Growth model in several hydrodynamic codes will continue to make it a very useful tool for shock initiation and detonation modeling and predictions for the foreseeable future.

ACKNOWLEDGEMENTS

The authors would like to thank Robert Druce and David Goosman for their Fabry-Perot records, David Aldis for the tantalum cylinder test report, and Albert Nichols for many helpful discussions concerning the ALE3D code.

*This work was performed under the auspices of the United States Department of Energy by the University of California, Lawrence Livermore National Laboratory under Contract No. W-7405-ENG-48.

REFERENCES

1. Dobratz, B. M., The Insensitive High Explosive TATB: Development and Characterization —1888 to 1994, Los Alamos National Laboratory Report LA-13014-H, UC-741, August 1995.
2. Tarver, C. M., Kury, J. W., and Breithaupt, R. D., J. Appl. Phys. **82**, 3771 (1997).
3. Tarver, C. M. and Hallquist, J. O., Seventh Symposium (International) on Detonation, NSWC MP 82-334, Annapolis, MD, 1981, p.488.
4. Ramsay, J. B., Eighth Symposium (International) on Detonation, Naval Surface Weapons Center NSWC 86-194, Albuquerque, NM, 1985, p. 372.
5. Tarver, C. M., Hallquist, J. O., and Erickson, L. M., Eighth Symposium (International) on Detonation, Naval Surface Weapons Center NSWC 86-194, Albuquerque, NM, 1985, p. 951.
6. Urtiew, P. A., Erickson, L. M., Aldis, D. F., and Tarver, C. M., Ninth Symposium (International) on Detonation, Office of the Chief of Naval Research OCNR 113291-7, Portland, OR, 1989, p. 112.
7. Bahl, K., Bloom, G., Erickson, L., Lee, R., Tarver, C., Von Holle, W., and Weingart, R., Eighth Symposium (International) on Detonation, Naval Surface Weapons Center NSWC MP 86-194, Albuquerque, NM, 1985, p. 1045.
8. Urtiew, P. A., Cook, T. M., Maienschein, J. L., and Tarver, C. M., Tenth International Detonation Symposium, Office of Naval Research, ONR 33395-12, Boston, MA, 1993, p. 139.
9. Urtiew, P. A., Tarver, C. M., Maienschein, J. L., and Tao, W. C., Combustion and Flame **105**, 43 (1996).
10. Tarver, C. M., Propellants, Explosives and Pyrotechnics **15**, 132 (1990).
11. Urtiew, P.A., Tarver, C. M., Forbes, J. W., and Garcia, F., Shock Compression of Condensed

Matter-1997, S. C. Schmidt, D. P. Dandekar, J. W. Forbes, eds., AIP Conference Proceedings 429, Woodbury, NY, 1998, p. 727.

12. Tarver, C. M., J. Phys. Chem. **101**, 4845 (1997).

13. Tran, T., Tarver, C., Maienschein, J., Lewis, P., Moss, M., Druce, R., Lee, R., and Roeske, F., Characterization of Detonation Wave Propagation in LX-17 near the Critical Diameter, paper presented at this Symposium.

14. Druce, R., Roeske, F., Fried, L., Souers, P. C., Tarver, C., Chow, C., Lee, R., McGuire, E., Overturf, G., Haskins, J., Schneberk, P., and Vitello, P., Propagation of Axially Symmetric Detonation Waves, paper presented at this Symposium.

15. Campbell, A. W. and Engelke, R., Sixth Symposium (International) on Detonation, Office of Naval Research ACR-221, Annapolis, MD, 1981, p. 642.

16. Campbell, A. W., Propellants, Explosives, Pyrotechnics **9**, 183 (1984).

17. Asay, B. W. and McAfee, Tenth International Detonation Symposium, Office of Naval Research, ONR 33395-12, Boston, MA, 1993, p. 485.

18. Gustavsen, R. L., Sheffield, S. A., Alcon, R. R., Forbes, J. W., Tarver, C. M., and Garcia, F., Shock Compression of Condensed Matter-2001, M. R. Furnish, ed., AIP Press, 2002, in press.

19. Price, D., J. Energetic Materials **1**, 55 (1983).

20. Steinberg, D. J. and Guinan, M. W., Lawrence Livermore National Laboratory Report No. UCRL-80465 (1978).

21. Tarver, C. M. and Maiden, D. E., Shock Waves in Condensed Matter — 1987, S. C. Schmidt, N. C. Holmes, eds., Elsevier Science B. V., 1988, p.363.

22. Aldis, D. F., Quirk, W., and Breithaupt, R. D., Lawrence Livermore National Laboratory Report UCRL-ID-107480, May 1991.

23. Goosman, D. R., Lawrence Livermore National Laboratory, private communication, 2001.

24. Neal, T., Sixth Symposium (International) on Detonation, Office of Naval Research ACR-221, Coronado, CA, 1976, p. 602.

25. Eden, G. and Belcher, R. A., Ninth Symposium (International) on Detonation, Office of the Chief of Naval Research OCNR 113291-7, Portland, OR, 1989, p. 831.

26. Nichols, A. L. III and Tarver, C. M., A Statistical Hot Spot Reactive Flow Model for Shock Initiation and Detonation of Solid High Explosives, paper presented at this Symposium.

TABLE 1. IGNITION & GROWTH PARAMETERS FOR LX-17, PBX 9502 AND EDC35

A. 25 °C LX-17		REACTION RATES	
UNREACTED JW	$\rho_0 = 1.905 \text{ g/cm}^3$		
A=632.07 Mbar	PRODUCT JW	$I = 4.0 \times 10^6 \mu\text{s}^{-1}$	
B=-0.04472 Mbar	A=14.8105 Mbar	$a = 0.22$	
$R_1 = 11.3$	B=0.6379 Mbar	$b = 0.667$	
$R_2 = 1.13$	$R_1 = 6.2$	$x = 7.0$	
$\omega = 0.8938$	$R_2 = 2.2$	$F_{\text{igmax}} = 0.02$	
$C_v = 2.487 \times 10^{-5} \text{ Mbar/K}$	$\omega = 0.50$	$G_1 = 1100 \text{ Mbar}^{-2} \mu\text{s}^{-1}$	
$T_0 = 298 \text{ K}$	$C_v = 1.0 \times 10^{-5} \text{ Mbar/K}$	$c = 0.667$	
Shear Modulus=0.0354 Mbar	$E_0 = 0.069 \text{ Mbar}$	$d = 1.0$	
Yield Strength=0.002 Mbar		$y = 2.0$	
		$F_{G1\text{max}} = 0.8$	
		$G_2 = 30 \text{ Mbar}^{-1} \mu\text{s}^{-1}$	
		$e = 0.667$	
		$z = 1.0$	
		$g = 0.667$	
		$F_{G2\text{min}} = 0.8$	
B. 25 °C PBX 9502		REACTION RATES	
UNREACTED JW	$\rho_0 = 1.895 \text{ g/cm}^3$		
A=632.07 Mbar	PRODUCT JW	$I = 4.0 \times 10^6 \mu\text{s}^{-1}$	
B=-0.04472 Mbar	A=13.6177 Mbar	$a = 0.214$	
$R_1 = 11.3$	B=0.7199 Mbar	$b = 0.667$	
$R_2 = 1.13$	$R_1 = 6.2$	$x = 7.0$	
$\omega = 0.8938$	$R_2 = 2.2$	$F_{\text{igmax}} = 0.025$	
$C_v = 2.487 \times 10^{-5} \text{ Mbar/K}$	$\omega = 0.5$	$G_1 = 1100 \text{ Mbar}^{-2} \mu\text{s}^{-1}$	
$T_0 = 298 \text{ K}$	$C_v = 1.0 \times 10^{-5} \text{ Mbar/K}$	$c = 0.667$	
Shear Modulus=0.0354 Mbar	$E_0 = 0.069 \text{ Mbar}$	$d = 1.0$	
Yield Strength=0.002 Mbar		$y = 2.0$	
		$F_{G1\text{max}} = 0.8$	
		$G_2 = 30 \text{ Mbar}^{-1} \mu\text{s}^{-1}$	
		$e = 0.667$	
		$z = 1.0$	
		$g = 0.667$	
		$F_{G2\text{min}} = 0.8$	
C. -54 °C PBX 9502 and LX-17			
$T_0 = 219 \text{ K}$	$\rho_0 = 1.895 \text{ g/cm}^3$		
B = -0.03928 Mbar		$G_1 = 900 \text{ Mbar}^{-2} \mu\text{s}^{-1}$	$G_2 = 30 \text{ Mbar}^{-1} \mu\text{s}^{-1}$
D. 75 °C PBX 9502 and LX-17			
$T_0 = 348 \text{ K}$	$\rho_0 = 1.895 \text{ g/cm}^3$		
B = -0.048162 Mbar		$G_1 = 1500 \text{ Mbar}^{-2} \mu\text{s}^{-1}$	$G_2 = 30 \text{ Mbar}^{-1} \mu\text{s}^{-1}$
E. 170 °C PBX 9502			
$T_0 = 443 \text{ K}$	$\rho_0 = 1.895 \text{ g/cm}^3$		
B = -0.0547 Mbar		$G_1 = 2000 \text{ Mbar}^{-2} \mu\text{s}^{-1}$	$G_2 = 30 \text{ Mbar}^{-1} \mu\text{s}^{-1}$
F. 250 °C PBX 9502			
$T_0 = 523 \text{ K}$	$\rho_0 = 1.895 \text{ g/cm}^3$		
B = -0.060206 Mbar		$G_1 = 2400 \text{ Mbar}^{-2} \mu\text{s}^{-1}$	$G_2 = 30 \text{ Mbar}^{-1} \mu\text{s}^{-1}$
G. EDC35		Other parameters — same as PBX 9502	
$T_0 = 298 \text{ K}$	$\rho_0 = 1.900 \text{ g/cm}^3$		

TABLE 2. EXPERIMENTAL & CALCULATED FAILURE DIAMETERS FOR PBX 9502 AND LX-17

EXPLOSIVE	To (BK)	FAILURE DIAMETER (mm)		GROWTH COEFFICIENTS	
		Experimental	Calculated	$G_1(y=2)(\text{Mbars}^2\mu\text{s}^{-1})$	$G_1(y=3)(\text{Mbars}^3\mu\text{s}^{-1})$
PBX 9502	298	>7 & <8	>7 & <8	1100	4200
PBX 9502	348	>5 & <6	>5 & <6	1500	7200
PBX 9502	219	>10 & <11	>10 & <11	900	3750
PBX 9502	443	>4 & <5**	>4 & <5	2000	7500
PBX 9502	523	>3 & <4**	>3 & <4	2400	8000
LX-17	298	~ 12	>11 & <12	1100	4200
LX-17	348		>8 & <9	1500	7200
LX-17	219		>15 & <16	900	3750

** Twice the failure thickness measured in the LANL Prism Test^{4,17}

TABLE 3. GRUNEISEN EQUATION OF STATE PARAMETERS FOR INERT MATERIALS

$$P = \rho_0 c^2 \mu [1 + (1 - \gamma_0/2) \mu - a/2 \mu^2] / [1 - (S_1 - 1) \mu - S_2 \mu^2 / (\mu + 1) - S_3 \mu^3 / (\mu + 1)^2]^2 + (\gamma_0 + a \mu) E,$$

where $\mu = (\rho/\rho_0 - 1)$ and E is thermal energy

INERT	$\rho_0(\text{g/cm}^3)$	$c(\text{mm}/\mu\text{s})$	S_1	S_2	S_3	γ_0	a
Al 6061	2.703	5.24	1.4	0.0	0.0	1.97	0.48
Steel	7.90	4.57	1.49	0.0	0.0	1.93	0.5
PMMA	1.186	2.57	1.54	0.0	0.0	0.85	0.0
Brass	8.45	3.834	1.43	0.0	0.0	2.0	0.0
Beryllium	1.85	8.0	1.124	0.0	0.0	1.11	0.16
Copper	8.93	3.94	1.489	0.0	0.0	2.02	0.47

TABLE 4. JONES — WILKINS — LEE (JWL) PARAMETERS FOR C-J DETONATION

- A. LX-16 (96% PETN, 4% FPC 461) $\rho_0 = 1.7\text{g/cm}^3$; $D = 0.7963\text{ cm}/\mu\text{s}$; $P_{CJ} = 0.30507\text{ Mbars}$; $A = 5.16784\text{ Mbars}$; $B = 0.24491\text{ Mbars}$; $R_1 = 4.5$; $R_2 = 1.5$; $\omega = 0.29$; $E_0 = 0.0986\text{ Mbar-cc/cc-g}$
- B. PBX 9407 (94% RDX, 6% Exon 461) $\rho_0 = 1.6\text{ g/cm}^3$; $D = 0.7910\text{ cm}/\mu\text{s}$; $P_{CJ} = 0.265\text{ Mbars}$; $A = 5.73187\text{ Mbars}$; $B = 0.14639\text{ Mbars}$; $R_1 = 4.6$; $R_2 = 1.4$; $\omega = 0.32$; $E_0 = 0.086\text{ Mbar-cc/cc-g}$
- C. Composition B $\rho_0 = 1.717\text{ g/cm}^3$; $D = 0.798\text{ cm}/\mu\text{s}$; $P_{CJ} = 0.295\text{ Mbars}$; $A = 5.242\text{ Mbars}$; $B = 0.07678\text{ Mbars}$; $R_1 = 4.2$; $R_2 = 1.1$; $\omega = 0.34$; $E_0 = 0.085\text{ Mbar-cc/cc-g}$

TABLE 5. COMPARISON OF DETONATION VELOCITIES AND ARRIVAL TIMES FOR EDC35 ALONG BRASS AND BERYLLIUM SLABS

Distance along Wall (mm)	Differences in Arrival Times: Experimental(μs)		Calculated (μs)	
0			0	
20			0.059	0.076
40			0.142	0.164
60			0.186	0.213
80			0.215	0.251
100			0.223	0.300
Average Detonation Velocities (mm/ μs)	Experimental: Brass	Beryllium	Calculated: Brass	Beryllium
	7.63 — 7.69	7.77 — 7.83	7.656	7.836